Heliyon 11 (2025) e42429

Contents lists available at ScienceDirect

Heliyon

journal homepage: www.cell.com/heliyon

Research article

Identifying macrophage-associated subtypes in patients with serous ovarian cancer and exploring potential personalized therapeutic drugs using combined single-cell and bulk RNA sequencing omics

Fei Teng [a,b], Hong Wei [a], Dehong Che [c], Kuo Miao [b], Xiaoqiu Dong [b,*]

[a] *In-Patient Ultrasound Department, The Second Affiliated Hospital of Harbin Medical University, Harbin, China*
[b] *Ultrasound Department, The Fourth Affiliated Hospital of Harbin Medical University, Harbin, China*
[c] *Ultrasound Department of Obstetrics and Gynecology, The Second Affiliated Hospital of Harbin Medical University, Harbin, China*

ARTICLE INFO

Keywords:
Serous ovarian cancer
Macrophage
Chemotherapy
Weighted gene co-expression network analysis
Marker

ABSTRACT

Purpose: We aimed to analyze the sensitivity of patients to chemotherapy drugs and actively explore potential new intervention targets, providing an essential reference for personalized treatment.

Methods: Candidate markers with significant differential expression in macrophages were identified by analyzing gene expression at the single-cell level. A weighted gene co-expression network (WGCN) was constructed on the GSE26712 dataset to explore the modules most relevant to macrophages. Differentially expressed genes for specific markers were identified. A multi-factor regulatory network was constructed based on single-cell dataset markers screening, differentially expressed genes, and genes commonly present in WGCNA modules. Different macrophage subtypes were identified using this network. Machine learning was used to filter and predict the markers' drug sensitivity, and the potential therapeutic compounds for specific markers were screened.

Results: We identified 14 and 17 of M1 and M2 macrophage candidate markers, respectively. In the multi-factor regulatory network of M1 macrophages, 6 out of 14 markers recognized 159 transcription factors (TFs) and 48 micro RNAs (miRNAs), whereas 13 of 17 markers recognized 191 TFs and 182 miRNAs in the multi-factor regulatory network of M2 macrophages. Filtering of the identified differentially expressed genes using random forests yielded 15 M1 and M2 macrophage-specific markers. Drug sensitivity prediction analysis and in vitro experiments revealed the close association of these markers with common chemotherapy drug sensitivity.

Conclusion: We identified specific M1 and M2 macrophage markers and found potential therapeutic compounds (dasatinib and afatinib) in these specific markers. These potential therapeutic compounds provide insight into the underlying mechanisms of serous ovarian cancer (OC) and inspire more effective treatment methods.

* Corresponding author.
E-mail address: Dongxq0451@163.com (X. Dong).

https://doi.org/10.1016/j.heliyon.2025.e42429
Received 29 May 2024; Received in revised form 14 January 2025; Accepted 31 January 2025
Available online 7 February 2025

1. Introduction

Ovarian cancer (OC) is a common and fatal malignancy affecting women's health globally [1]; its mortality and morbidity rate ranks third and fourth, respectively [1]. Serous OC is the most common cause of death among patients with OC. Continuous ovulation, low immune system function, abnormal hormone levels, and reactive oxygen species production are causes of OC [2]. Despite unprecedented advances in OC diagnosis and treatment, patient prognosis remains unclear. The 5-year survival rate of OC is <50 %, much lower than that of breast cancer (85 %) [3]. Identifying and regulating new risk factors for OC occurrence, development, metastasis, and invasion is significant for early diagnosis and personalized intervention. Therefore, finding new OC prognostic markers and further study of new intervention targets is essential to improve the accurate prediction of OC prognosis and provide a scientific basis for clinical decision-making.

The tumor microenvironment (TME) is vital in cancer initiation and progression [4]. There are many types of cells in the TME of serous OC, including myeloid derived suppressor cells, T lymphocytes, natural killer cells, macrophages, neutrophils, cancer-related fibroblasts, and tumor cells [5]. Notably, several TME immune infiltrating cells interact with tumor cells, such as natural killer cells [6,7], cytotoxic T cells [8,9], and CD8+T cells [10], which play anti-tumor roles. Immunosuppressive cells such as fibroblasts [11,12] and myeloid derived suppressor cells [13–15] play a role in tumor promotion. In addition, Li et al. found that M2 macrophages increased OC resistance to cisplatin [16], whereas Wanderley et al. showed that M1 macrophages inhibited tumor growth by increasing their sensitivity to porphyrosol [17]. Previous studies have shown that M1 and M2 macrophages are associated with the clinical outcomes of patients with OC [18,19]. Therefore, identifying new prognostic markers and intervention targets based on M1 and M2 macrophages in patients with OC is important.

Recently, single-cell RNA sequencing (scRNA-seq) has rapidly developed, providing an essential basis for the further analysis of tumors at the cellular level. scRNA-seq also provides unprecedented insights into stromal and immune cell diversity in the TME [20]. The TME has been described at the single-cell level for many cancers, including melanoma [21], lung cancer [22], head and neck cancer [23], hepatocellular carcinoma [24], glioma [25], medulloblastoma [26], and pancreatic cancer [27]. However, only a few studies have elucidated TME composition in patients with OC, and an in-depth description of the immune cell composition in the TME of these patients is needed urgently.

This study synthesized bulk RNA-seq and scRNA-seq gene expression profiles for serous OC to classify patients with OC by screening candidate markers for M1 and M2 macrophages. Simultaneously, we analyzed the sensitivity of patients to chemotherapy drugs and actively explored potential new intervention targets, providing an essential reference for personalized treatment. These findings strongly support precision medicine development and novel treatment strategies for patients with OC.

2. Materials and methods

2.1. Patients

All tumor and normal tissue samples of patients with serous OC were obtained from the Second Affiliated Hospital of Harbin Medical University. The paired tissue specimens from 10 patients were collected. This study was approved by the Clinical Research Ethics Committee of the Second Affiliated Hospital of Harbin Medical University.

2.2. Data downloading and preprocessing

Bulk RNA-seq and scRNA-seq gene expression profiles of two sets of serous OC, GSE26712 [28] and SOL2095 [29] were downloaded from the gene expression omnibus (GEO) database and previous literature, as shown in Table 1. The Robust multichip average algorithm in the R package "affy" was used to process and standardize the dataset for bulk RNA-seq gene expression profiles, and the probe ID was converted to the gene name using the corresponding platform annotation file. The probe with the highest expression level was selected for each sample if multiple probes corresponded to the same gene.

2.3. scRNA-seq data analysis

The scRNA-seq data was converted into Seurat objects using the R package "Seurat." Quality control of the scRNA-seq data was performed using three strategies: retaining only genes expressed in at least five cells, removing cells expressing <100 genes, and removing >5 % of the mitochondrial genes. The "NormalizeData" function was used to normalize the scRNA-seq data, and the "FindVariableFeatures" function was used to identify the first 2000 highly variable genes. Furthermore, the "RunPCA" function was used for principal component analysis. Data dimensionality was reduced based on the first 2000 genes, and the first 15 principal components were selected for cell cluster analysis. The "FindAllMarkers" function was used to calculate each cluster's differentially

Table 1
Gene expression profile data of serous ovarian cancer.

Dataset ID	Platform	Sample Size
GSE26712	GPL96	195
SOL2095	NA	12

expressed genes (DEGs). The threshold criteria for differential epigenetic genes were adjusted at $P < 0.05$ and $|\log2 \text{ (fold change)}| > 0.25$. We manually annotated each cluster cell type.

2.4. Cell-type identification by estimating relative subsets of ribonucleic acid transcripts deconvolution analysis

We quantified the proportion of 22 types of immune cells in the bulk RNA-seq gene expression profiles using Cell-type Identification by Estimating Relative Subsets of Ribonucleic acid Transcripts (CIBERSORT). This algorithm estimates the relative proportion of 22 types of immune cells based on gene expression profiles. To run CIBERSORT, we downloaded the LM22.txt file from the website (https://cibersort.stanford.edu/download.php), a "signature matrix" containing 547 genes and 22 types of immune cells.

2.5. Weighted gene co-expression network analysis

Weighted gene co-expression network analysis (WGCNA) is a systems biology approach that identifies highly related gene modules based on gene sets and phenotype associations, searching for candidate biomarker genes and potential therapeutic targets. This study constructed WGCNA by selecting gene expression profiles. The samples and genes were filtered, and Pearson's correlation between all gene pairs in the selected samples was calculated using the R-package "WGCNA" to construct the adjacency matrix. Then, $\beta = 10$ (scale-free $R^2 = 0.90$) was used as a soft threshold, ensuring a scale-free network. The functional modules in the WGCNA were identified by calculating the topological overlap metric (TOM) using an adjacency matrix. Gene modules and Screen module feature genes (ME) were established through a dynamic-tree building method based on the TOM values. The MEs were considered representative of the gene expression profiles in the module.

2.6. Construction of the competitive endogenous RNA regulatory network

Transcription factors (TFs) were downloaded from joint analysis of splice sites (JASPAR) and human TF (hTF) target databases, and the intersection of TFs from the two databases was used for TF preliminary screening. Candidate markers, micro RNAs (miRNAs), and TFs were associated based on the TargetScan database, and a multi-factor regulatory network was constructed.

2.7. Unsupervised clustering, differential expression, and enrichment analysis

Bulk RNA-seq gene expression profiles were classified using unsupervised clustering. It was performed using the R package "ConsensusClusterPlus," which is based on a computational consensus clustering method. Consensus clustering provides quantitative evidence to determine the number of potential clusters in a gene expression profile. This study used the "ConsensusClusterPlus" function to cluster the bulk RNA-seq gene expression profiles of 185 serous OC samples from GSE26712. The main parameters used in the analysis are clusterAlg = "hc," distance = "pearson."

Differential expression analysis of dataset GSE26712 was performed using "limma," and the threshold criteria were $|\log2FC| > 0.5$ and $P < 0.05$.

Enrichment analysis of Gene Ontology (GO) and Kyoto encyclopedia of genes and genomes (KEGG) [30,31] was achieved using enrichGO and enrichKEGG functions in the R package "clusterProfiler," respectively.

2.8. Random forest classification

Differentially expressed genes were classified using Random Forest analysis and R package "randomforest." First, the optimal number of variables (mtry parameter, the optimal number of variables used by the binary tree on the specified node) was determined. All possible variables were looped into the random forest classifier, each error rate was calculated, and the optimal number of variables was selected. The error rates of 1–200 trees were calculated, and the optimal number of trees (ntree = 50) was the number of trees with the lowest error rate and best stability. Based on the selected parameters, the random forest classifier was used to calculate the results, and the genes were sorted according to the Mean Decrease Accuracy and Mean Decrease Gini coefficients; essential genes were selected as candidate-specific genes.

2.9. Drug sensitivity prediction analysis

Based on the maximum of pharmacogenomics database - Genomics of Drug Sensitivity in Cancer (GDSC, https://www.cancerrxgene.org/), the chemical sensitivity of each tumor sample was predicted using the R package "oncoPredict" and the semi-inhibitory concentration (IC50) of each specific chemotherapy agent was assessed using regression, with all parameters selected as default values.

2.10. Cell culture and quantitative reverse transcriptase polymerase chain reaction

Human ovarian cell lines, including embryonic stem cells-2, OVKATE, OAW28, A2780, and OV-90, and a regular ovarian cell line (IOSE-80), were procured from ATCC (Manassas, VA, USA). The ovarian cell lines were cultured in Ham's F-12K medium (Jiangsu Kaiji Biotechnology Co., Ltd, Wuxi, China) or Roswell Park Memorial Institute-1640 medium (Gibco Laboratories, Grand Island, NY, USA),

whereas IOSE-80 cells were maintained in Dulbecco's Modified Eagle Medium (Gibco Laboratories).

Total RNA was extracted and reverse-transcribed using TRIzol reagent (Invitrogen, Carlsbad, CA, USA) and a complementary deoxyribonucleic acid reverse transcription kit (Applied Biosystems, Foster City, CA, USA) according to the manufacturer's instructions. Quantitative reverse transcriptase polymerase chain reaction (qRT-PCR) was performed using the SYBR Green reagent (Thermo Fisher Scientific, Waltham, MA, USA). The relative expression of target genes was calculated using the $2^{-\Delta\Delta CT}$ method, and β-actin was used as the internal reference. Supplementary Table S1 lists the primer sequences.

2.11. Western blotting and cell counting Kit-8 assay

Western blot analysis was performed to determine the protein expression levels of Matrix Remodeling Associated 8 (MXRA8) and Ubiquitin-Specific Protease 34 (USP34). Proteins were separated using sodium dodecyl sulfate-polyacrylamide gel electrophoresis and transferred onto a polyvinylidene fluoride membrane with anti-MXRA8 (1:1000; Cell Signaling Technology, Danvers, MA, USA; 4273S). Primary antibodies to USP34 (1:1000, Cell Signaling Technology, 8581) and glyceraldehyde-3-phosphate dehydrogenase (ZSBG-Bio; TA-6) were incubated overnight at 4 °C. After incubation with horseradish peroxidase-conjugated secondary antibodies for 2 h, signals were visualized using enhanced chemiluminescence (Beyotime, Beijing, China).

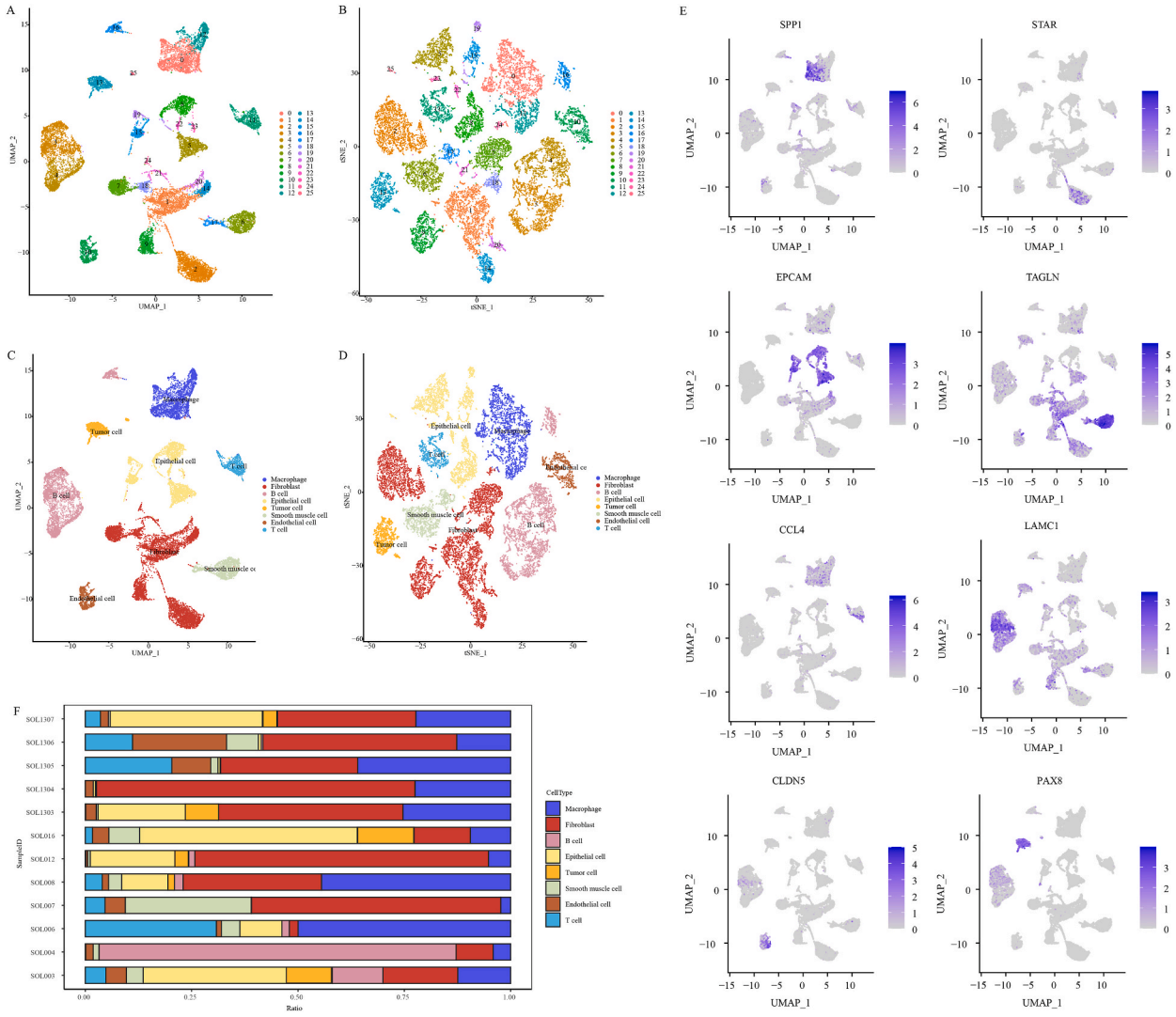

Fig. 1. Analysis of serous OC single-cell data. a, UMAP plot showing 18,403 high-quality cells according to cell cluster. b, t-SNE plot showing 18,403 high-quality cells according to cell cluster. c, UMAP plot showing 18,403 high-quality cells according to cell type. d, t-SNE plot showing 18,403 high-quality cells according to cell type. e, UMAP diagram shows the specific markers of seven immune cell types. f, Histogram showing the relative proportions of seven immune cell types in each sample. UMAP, uniform manifold approximation and projection; t-SNE, t-distributed stochastic neighbor embedding.

The cells were implanted in 96-well microplates and treated with 0.01 nmol/mL of dasatinib and 0.1 nmol/mL of afatinib for 24, 48, or 72 h. Furthermore, 10 μL cell counting kit-8 (CCK-8) solution (Dojindo Laboratories, Mashiki, Japan) was added to each well and incubated at 37 °C for 2 h, and the optical density value was determined at 450 nm.

2.12. Colony formation assay

A 2-mL medium containing 0.4 % AGAR was used as the base gel. Next, 1000 cells were suspended in 4 mL of 0.2 % AGAR medium and poured onto the bottom gel. After 2 weeks, the colonies were stained with 3-(4,5-dimethylthiazol-2-yl)-2,5-diphenyltetrazolium bromide. The colonies were counted under a microscope at low power. Colony size was analyzed using Colony Counter software (Tanon; BioTanon, Shanghai, China), and 0.01 nmol/mL of dasatinib or 0.1 nmol/mL of afatinib was added [32].

2.13. Immunohistochemistry

Immunohistochemistry (IHC) was conducted following the established protocol. Tissue sections were incubated overnight at 4 °C with a rabbit polyclonal anti-MXRA8 antibody (Cat. No. ab134356; 1:100 dilution; Abcam, Cambridge, UK) and a rabbit polyclonal anti-USP34 antibody (Cat. No. ab167538; 1:100 dilution; Abcam). Afterward, the sections were washed with phosphate-buffered saline and subsequently incubated with biotinylated secondary antibodies (Cat. No. 107-037-052, No. 121-013-061; 1:1500 dilution; Jackson ImmunoResearch, West Grove, PA, USA) at room temperature for 30 min. Diaminobenzidine was then applied for 5 min at room temperature to visualize the staining. A negative control was prepared by repeating the procedure with phosphate-buffered saline instead of the primary antibody. Further details can be found in Supplementary Table S2.

2.14. Statistical analysis

The surv_cutpoint function in the R package “survminer” was used to calculate the best truncation value and group the patients. At the same time, Kaplan–Meier survival curves between different patient groups were plotted based on R package “survminer” and “Survival,” and a bilateral Log-rank test was performed to determine the significance of differences. The R package “ggplot2” was used for the drawings.

All statistical analyses were performed using the R programming language (version 4.2.0; R Foundation for Statistical Computing, Vienna, Austria). Unless otherwise stated, statistical significance was set at two-sided $P < 0.05$.

3. Results

3.1. Screening candidate markers for macrophages based on single-cell data

The scRNA-seq dataset SOL2095 of serous OC was obtained from previous studies, and quality control was performed, resulting in 33,694 genes and 18,403 cells. After performing dimensionality reduction and clustering analysis on the dataset SOL2095, we placed 18,403 cells into 26 clusters (Fig. 1a and b) and identified seven immune cell types (Fig. 1c and d), including macrophages, fibroblasts, B cells, epithelial cells, smooth muscle cells, endothelial cells, and T cells. Fig. 1e shows the expression markers for each immune cell type. We also analyzed the proportions of various immune cells in each sample, and the composition of immune cells showed heterogeneity between samples (Fig. 1f). After identifying immune cells, we conducted a differential expression analysis and found that macrophages had 1939 differentially expressed genes compared with other immune cells (Supplementary Table S3). Furthermore, the DEGs of other immune cells are shown in Supplementary Table S4.

We used SCENIC to analyze transcription factor activity and evaluate differences in activity across various cell types. The results revealed that transcription factors such as MAFK and MYBL2 exhibited significantly increased activity in tumor cells, suggesting their potential roles in regulating tumor cell proliferation and metabolism (Supplementary Fig. 1a). In addition, we conducted cell-cell interaction analysis, which revealed complex communication networks between different cell types. Notably, the interactions between tumor cells and macrophages were particularly prominent, potentially linked to immune suppression and extracellular matrix remodeling within the tumor microenvironment (Supplementary Figs. 1b–c). Furthermore, the extensive interactions between epithelial and endothelial cells may reflect mechanisms related to angiogenesis or barrier function regulation. Ligand-receptor dot plot analysis further illustrated key signaling pathways between specific cell types. The interactions between tumor cells and macrophages were primarily mediated through signaling pathways such as CDH1-KLRG1 and JAG1-NOTCH1, which are likely associated with immune evasion (Supplementary Fig. 1d).

3.2. Macrophage infiltration landscape in patients with serous ovarian cancer

Based on the CIBERSORT algorithm, deconvolution analysis was performed on 185 serous OC samples from the bulk RNA-seq dataset GSE26712 to calculate the relative abundances of 22 immune cells. Furthermore, we calculated the optimal cut-off value for the relative abundance of M1 and M2 macrophages and grouped patients accordingly. We analyzed the survival differences between patients with high and low abundance. Patients with high abundance in the group based on M1 macrophage relative fractionation had a better prognosis (Supplementary Fig. 2a). However, patients with high abundance in the group based on M2 macrophage relative fractionation had a shorter outcome (Supplementary Fig. 1b). The GEO in The Cancer Genome Atlas database was

used for verification to ensure reliable result analysis, and the results showed a similar trend (Supplementary Figs. 2c and d).

3.3. WGCNA identifies candidate markers for macrophage subtypes

WGCNA was performed on 185 tumor samples from the GSE26712 dataset to obtain candidate markers for M1 and M2 macrophages. We chose the optimal $\beta = 10$ to ensure a scale-free network (Fig. 2a). The next step was to convert the expression matrix into an adjacency matrix and then convert the adjacency matrix into a topology matrix. Based on TOM, genes were clustered using the average-linkage hierarchical clustering method based on the standard of hybrid dynamic shear trees, and the gene network module minimum number of genes was set at 20. After using the dynamic shearing method to determine the gene modules, we calculated the eigengenes of each module, performed a cluster analysis on the modules, and merged the modules closer into new modules, resulting in nine modules (Fig. 2b).

Furthermore, the correlation between each module and the relative abundance of M1/M2 macrophages was calculated (Fig. 2c). The green module had the highest correlation coefficient with the relative abundance of M1 macrophages (Fig. 2d). However, the yellow module had the highest correlation coefficient with the relative abundance of M2 macrophages (Fig. 2e). GO and KEGG enrichment analysis was performed on 75 and 119 genes in the green and yellow modules, respectively, and the results showed that these genes were mainly enriched in oncogenic and metabolism-related pathways (Fig. 2f–i).

Differentially expressed genes were detected in 10 normal and 185 tumor tissue samples in dataset GSE26712; 1078 genes were highly expressed in patients with serous OC, whereas 647 were expressed at low levels (Fig. 2j).

However, the macrophage candidate markers, differentially expressed genes, M1 macrophage markers, and M2 macrophage markers identified using WGCNA overlapped based on single-cell data screening, and 14 M1 (Fig. 2k–Supplementary Table S5) and 17 M2 macrophage candidate marker genes (Fig. 2l–Supplementary Table S5) were obtained.

3.4. Constructing a multi-factor regulatory network based on candidate macrophage markers

A multi-factor regulatory network was constructed using 14 M1 and 17 M2 macrophage candidate marker genes. First, TFs were downloaded from JASPAR and hTFTarget databases. In total, 888 and 495 TFs were obtained from JASPAR and hTFTarget databases, respectively. TF intersection in the two databases yielded 216 TFs. Based on the Target scan database, we explored the miRNAs and TFs interacting with the candidate markers and associated miRNAs, TFs, and macrophage candidate markers to build a multi-factor regulatory network. The M1 macrophage multi-factor regulatory network contained six M1 macrophage candidate markers (green), 159 TFs (red), and 48 miRNAs (blue) (Supplementary Fig. 3a, Supplementary Table S6). The M2 macrophage multi-factor regulatory network contains 13 M2 macrophage candidate markers (yellow), 191 TFs (red), and 182 miRNAs (blue) (Supplementary Fig. 3b, Supplementary Table S7).

3.5. Identifying different M1 and M2 macrophage subtypes

Patients in the dataset GSE26712 were clustered based on 6 and 13 candidate markers for M1 and M2 macrophages, respectively. The clustering results showed that when the number of clusters was three, there were obvious differences between the samples (Fig. 3a and b). The difference between patients with the S1, S2, and S3 subtypes was more significant in the heatmap of the six candidate markers (Fig. 3c). The clustering results of the 13 candidate markers based on M2 macrophages showed noticeable differences between the samples when the number of clusters was three (Fig. 3d and e). A significant difference between patients with the S1 subtype and those with the S2/S3 subtype was found in the heatmap of the 13 candidate markers (Fig. 3f).

3.6. Screening specific markers for M1 and M2 macrophage subtypes

Based on the consensus clustering results, we performed differential expression analysis on patients with M1 and M2 macrophage subtypes and screened for differentially expressed genes in the subtypes. Among patients with the M1 macrophage subtype, the differentially expressed genes between S1/S2 and S3 patients were compared, and 167 differentially expressed genes were identified (Fig. 4a), of which 39 that were significant in the S1/S2 subtype were upregulated (Fig. 4b). We compared the differentially expressed genes between S1 and S2/S3 subtypes in patients with M2 macrophage subtypes and identified 851 differentially expressed genes (Fig. 4c), of which 33 were significantly upregulated in the S1 subtype. (Fig. 4d). We further used the random forest algorithm to screen 39 and 33 differentially expressed and upregulated genes in M1 and M2 macrophages, respectively. The weight of each gene was calculated using RandomForest, and the top 30 genes were selected based on the Gini coefficient and accuracy. Finally, 15 genes were identified as specific M1 and M2 macrophage markers (Fig. 4e–h). Fig. 4 (i and j) shows the difference in the specific marker expression of M1 and M2 macrophages in tumor tissues and normal tissues, respectively. We found that the expression of some genes, such as *MXRA8* and *USP34*, differed significantly between the tumor and normal tissues.

3.7. Revealing the relationship between M1 and M2 macrophage-specific markers and drug sensitivity

The GDSC database was used to predict each patient's sensitivity to common chemotherapy drugs in the GSE26712 dataset. Furthermore, the correlation between drug sensitivity and M1 and M2 macrophage-specific markers' expression levels was analyzed. Supplementary Fig. 4 (a and b) shows the correlation coefficients between M1 and M2 macrophage-specific markers and their

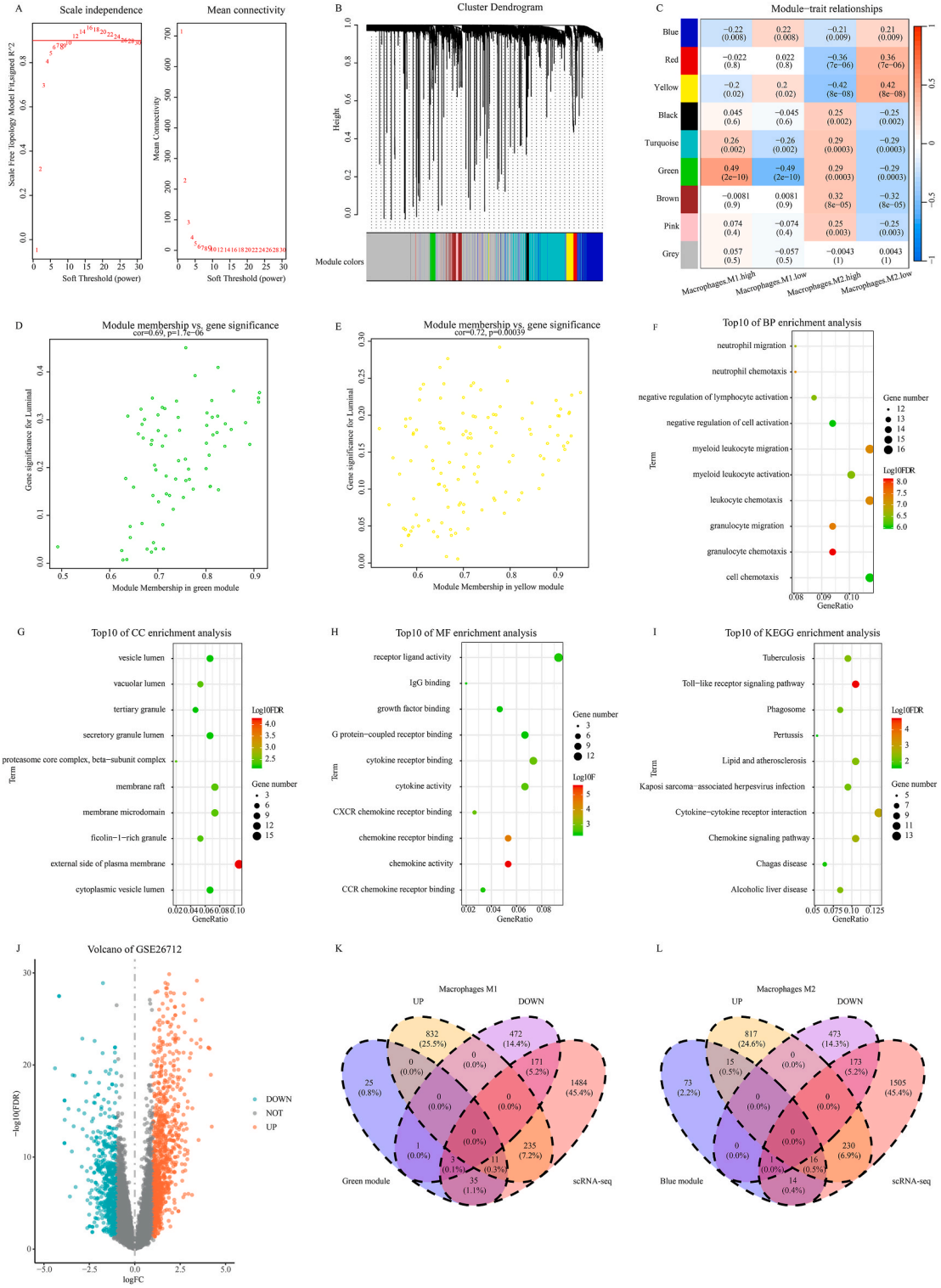

Fig. 2. Candidate markers for identifying macrophage subtypes. a. Soft threshold analysis method is used to obtain the scale-free fitting index of the network topology. b, Hierarchical clustering analysis is used to detect co-expression clusters with corresponding color assignments, with each color representing a module in the gene co-expression network constructed by WGCNA. c, Correlation between genes in different modules and M1 or M2 macrophages. d, Analysis of gene significance and module membership in green modules. e, Analysis of gene significance and module membership in the yellow module. f, Bubble chart shows the top 10 pathways in biological process (BP) enrichment analysis of green and yellow module genes. g, Bubble chart showing the top 10 pathways in cellular component (CC) enrichment analysis of green and yellow module genes. H, Bubble chart

showing the top 10 pathways in molecular function (MF) enrichment analysis of green and yellow module genes. i, Bubble chart showing the top 10 pathways in KEGG enrichment analysis of green and yellow module genes. j, Volcano plot of differentially expressed genes in dataset GSE26712. k, Venn diagram of macrophage candidate markers screened by single-cell data, differentially expressed genes, and M1 macrophage markers identified using WGCNA. l, Venn diagram of macrophage candidate markers screened using single-cell data, differentially expressed genes, and M2 macrophage markers identified using WGCNA. KEGG, Kyoto encyclopedia of genes and genomes; WGCNA, weighted gene co-expression network analysis.

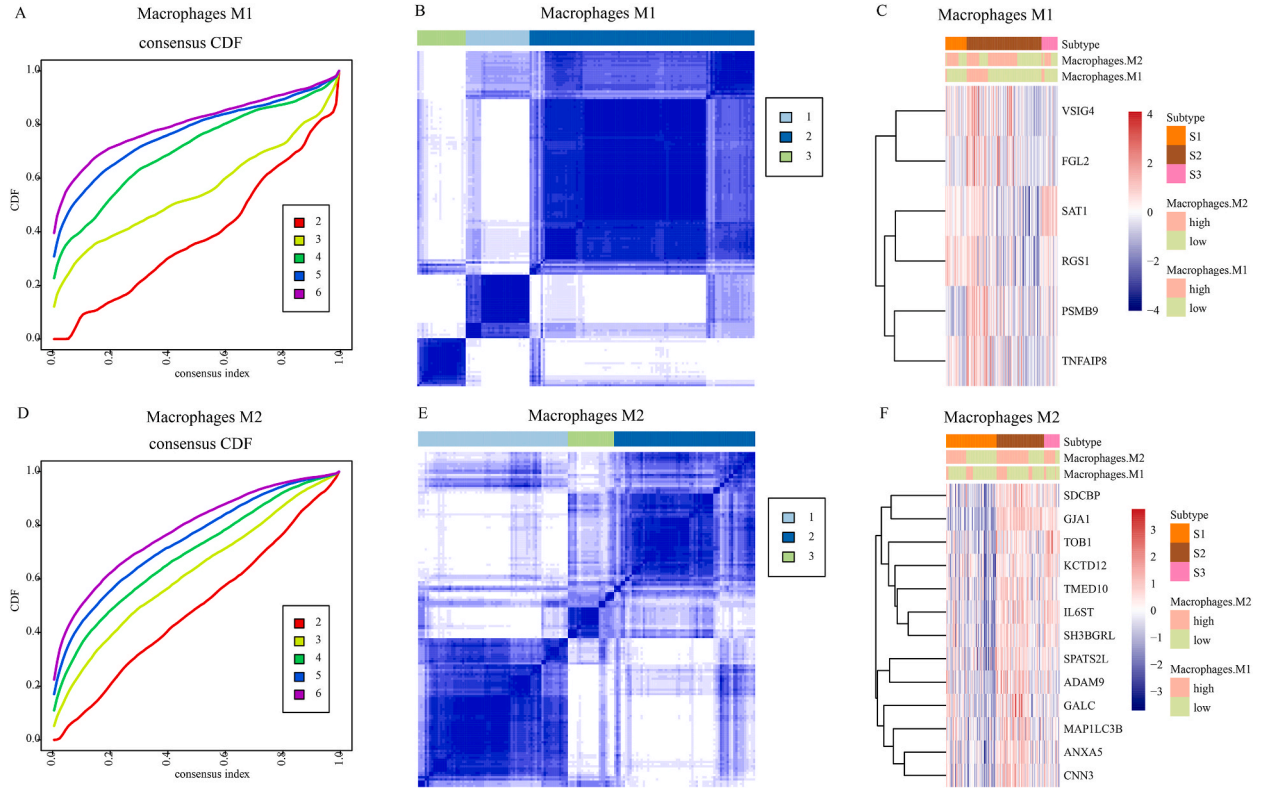

Fig. 3. Classification of patients using candidate markers of macrophages. a, Consensus clustering cumulative distribution function (CDF) based on candidate markers of M1 macrophages when k = 2–6. b, Consensus clustering matrix of 185 serous ovarian cancer samples at k = 3 based on candidate markers for M1 macrophages. c, Heat map of six candidate markers based on the consistent clustering results of M1 macrophages. d, Consensus clustering cumulative distribution function (CDF) based on candidate markers of M2 macrophages when k = 2–6. e, Consensus clustering matrix of 185 serous ovarian cancer samples at k = 3 based on candidate markers of M2 macrophages. f, Heat map of 13 candidate markers based on the consistent clustering results of M2 macrophages.

sensitivity to common chemotherapeutic drugs. We observed that the expression levels of some markers were negatively correlated with chemotherapy drug sensitivity, such as *MXRA8* expression levels and dasatinib sensitivity and *USP34* expression levels and afatinib sensitivity.

The intervention targets of M1 and M2 macrophage-specific markers were identified by constructing a univariate Cox proportional risk model using specific markers, which analyzed their impact on the prognosis of patients with serous OC. As a specific marker of M1 macrophages, *MXRA8* significantly impacted patient prognosis and was a risk factor in patients with serous OC (Supplementary Fig. 4c). Notably, the specific markers of M2 macrophages, Disco-Interacting Protein 2 Homolog A (*DIP2A*) and *USP34*, had a significant impact on patient prognosis and were risk factors in patients with serous OC (Supplementary Fig. 4d). In the Kaplan–Meier survival analysis of the validation dataset, *MXRA8* was also unfavorable for patient prognosis(Supplementary Fig. 4e). In the survival analysis of the validation dataset TCGA, *USP34* was unfavorable for patient prognosis, whereas *DIP2A's* impact on patient survival was not significant (Supplementary Fig. 4f).

3.8. In vitro experiments have confirmed that M1 and M2 macrophage-specific markers are resistant to dasatinib and afatinib

We conducted in vitro experiments to confirm the reliability of these results. First, we analyzed *MXRA8* and *USP34* differential expression in multiple and normal OC cell lines. *MXRA8* and *USP34* were upregulated in OC cell lines (Fig. 5a). We transfected si-MXRA8 and si-USP34 into OAW28 and A2780 cell lines, respectively, and found that *MXRA8* and *USP34* expression was significantly reduced (Fig. 5b). Western blotting revealed similar results (Fig. 5c).

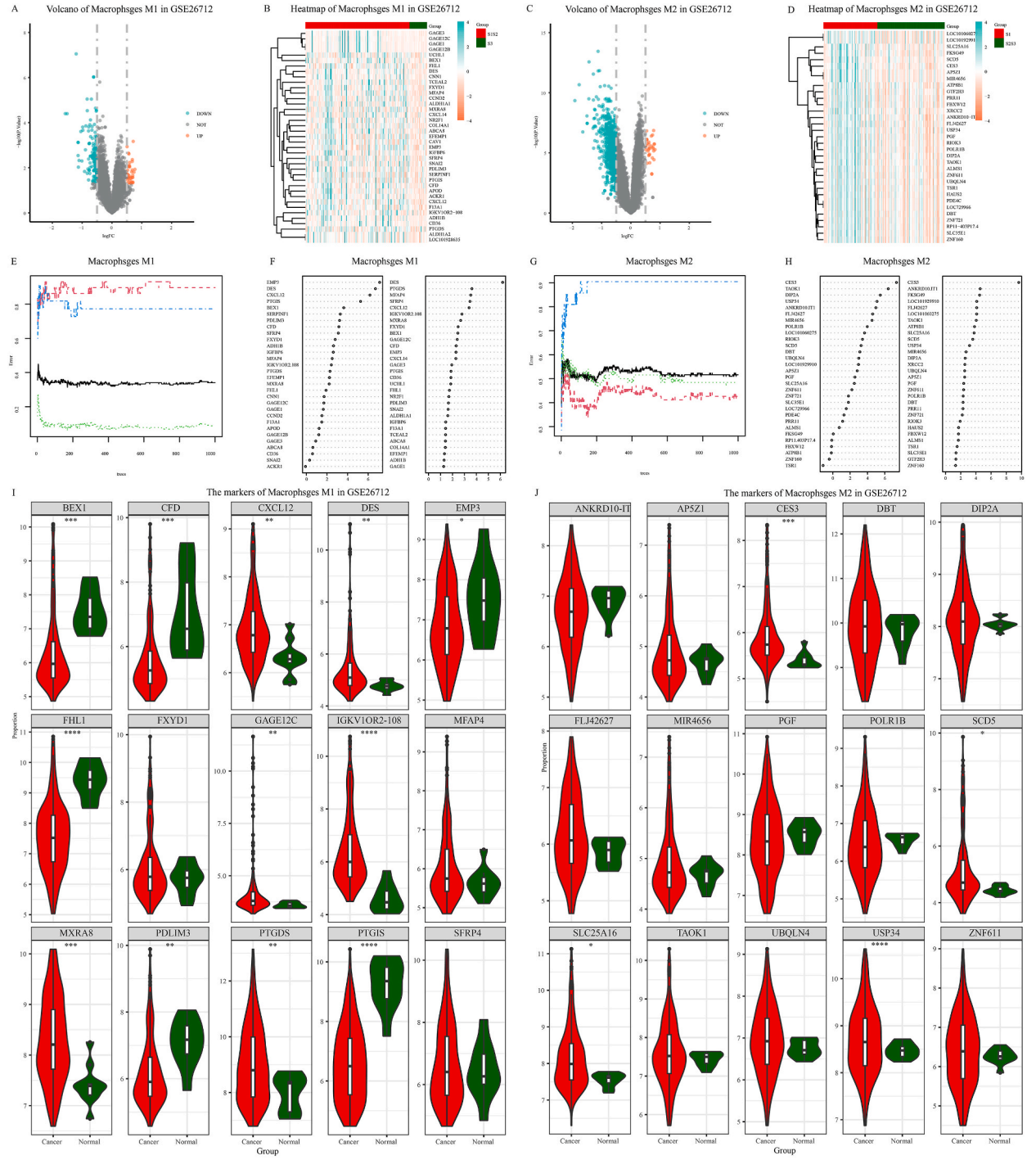

Fig. 4. Specific markers for M1 and M2 macrophages. a, Volcano plot of differentially expressed genes based on M1 macrophage grouping. b, Heat map of differentially expressed genes based on M1 macrophage grouping. c, Volcano plot of differentially expressed genes based on M2 macrophage grouping. d, Heat map of differentially expressed genes based on M2 macrophage grouping. e, Out-of-bag (OOB) error rate assessing the quality of random forest predictions in patients with M1 macrophage subgroups. f, The importance of differentially upregulated genes in M1 macrophage grouping patients calculated based on random forest and rank them, and the top 30 genes selected. g, OOB error rate assessing the quality of random forest predictions in patients with M2 macrophage subgroups. h, The importance of differentially upregulated genes in M2 macrophage grouping patients calculated based on random forest, ranked, and the top 30 most important genes selected. i, Differences in the expression of specific markers of M1 macrophages in tumor and normal tissues. j, Differences in the expression of specific markers of M2 macrophages in tumor and normal tissues.

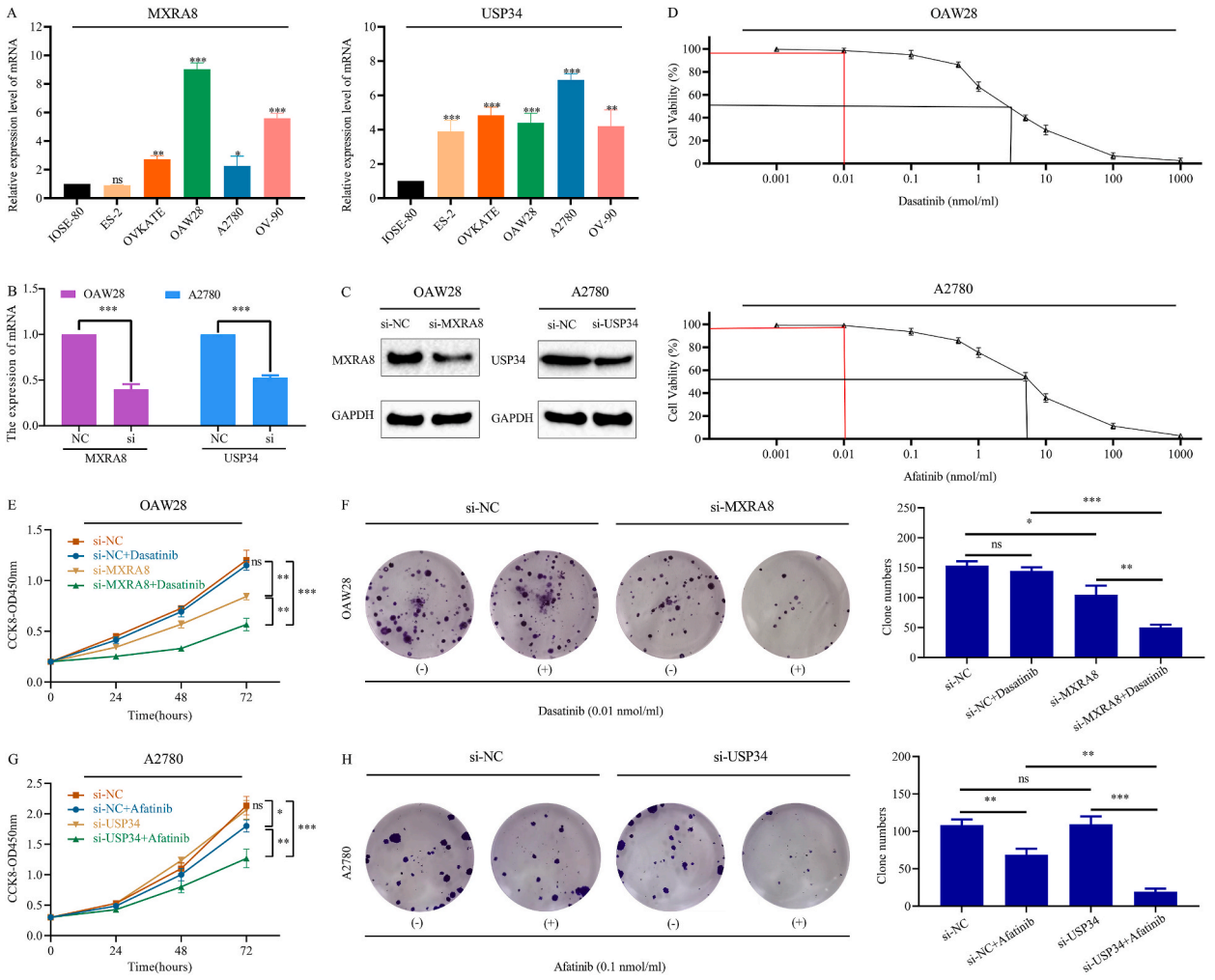

Fig. 5. In vitro experimental verification analysis results. a, qRT-PCR analysis detects the expression of MXRA8 and USP34 in the normal ovarian epithelial cell line IOSE-80 and five OC cell lines. b, qRT-PCR analysis detects the knockdown efficiency of MXRA8 and USP34 at the RNA level in OC cell lines OAW28 and A2780, respectively. c, Western blotting detects the knockdown efficiency of MXRA8 and USP34 protein levels in OC cell lines OAW28 and A2780, respectively. d, CCK-8 experiment detects the changes in dasatinib and afatinib cell viability under different concentrations of OAW28 and A2780, IC50 (black line), and initial inhibitory concentration (red line). e, CCK-8 experiment detects changes in OAW28 proliferation levels under different treatment conditions. f, Colony formation assay is used to detect the effects of different treatment conditions on OAW28 proliferation levels. g, CCK-8 experiment detects changes in A2780 proliferation levels under different treatment conditions. h, Colony formation assay is used to detect the effects of different treatment conditions on the proliferation level of A2780. qRT-PCR, quantitative reverse transcriptase-polymerase chain reaction; MXRA8, Matrix Remodeling Associated 8; USP34, Ubiquitin-Specific Protease 34; OC, ovarian cancer; IC50, semi-inhibitory concentration.

Furthermore, we validated *MXRA8* and *USP34* sensitivity to dasatinib and afatinib, respectively. We investigated the relationship between the cytotoxic effects of dasatinib on OAW28 and afatinib on A2780 cells and changes in drug concentration by setting a concentration gradient from 0.001 to 1000 nmol/mL so that OAW28 and A2780 cells were simultaneously treated at different drug concentrations. The cell viability values were calculated and compared with those of the blank control group. The results indicated that the IC_{50} values of dasatinib-OAW28 and afatinib-A2780 were between 1 and 10 nmol/mL (Fig. 5d, black line). Notably, when dasatinib was 0.01 nmol/mL, OAW28 cell viability was initially inhibited (Fig. 5d, top red line). Similarly, when afatinib was 0.1 nmol/mL, A2780 cell viability initially showed inhibition (Fig. 5d, bottom, red line). We selected 0.01 nmol/mL of dasatinib and 0.1 nmol/mL of afatinib as drug concentrations for further studies. We further validated the relationships between MXRA8, OAW28, dasatinib, USP34, A2780, and afatinib. In OAW28 cells, MXRA8 was resistant to dasatinib (Fig. 5e), as confirmed by colony formation experiments (Fig. 5f). In the A2780 cell line, USP34 showed similar results for afatinib (Fig. 5g and h).

In addition, to further validate the expression levels of *MXRA8* and *USP34*, we collected tissue samples from 10 patients with serous OC. The expression of *MXRA8* and *USP34* in clinical specimens of cancer patients was detected using qRT-PCR method. The results showed that *MXRA8* and *USP34* were strongly expressed in serous OC tissues (Supplementary Figs. 4a and b), and IHC analysis of

MXRA8 and USP34 also showed a similar trend (Supplementary Figs. 5c–g). Besides, we also used immunofluorescence staining to analyze the expression levels of MXRA8 and USP34 in M1 and M2 macrophages, respectively. The results showed that MXRA8 and USP34 had higher expression levels in M1 and M2 macrophages, respectively (Supplementary Figs. 6a–b).

4. Discussion

The clinical outcomes in patients with serous OC have significant patient specificity, with a survival time from 5 months to >10 years [33]. Radical surgery and chemotherapy are the primary treatment measures for patients with serous OC, which significantly prolong the interval between relapses. However, patients' overall survival rates have not improved significantly [34]. Therefore, new drug targets for treating patients with OC to prolong their survival are necessary. Notably, some recognized clinical phenotypes, such as tumor staging and grading, have been widely used to guide patients on whether to receive adjuvant chemotherapy after surgery. However, they cannot fully distinguish patients at an increased risk of tumor progression [35]. Therefore, more focus should be on exploring new classification methods to stratify patients and provide personalized treatment.

This study identified candidate markers for macrophages using single-cell gene expression profiles of serous OC and performed deconvolution analysis and WGCNA on bulk RNA-seq gene expression profile data using CIBERSORT to identify candidate markers associated with M1 and M2 macrophages. We analyzed differential expression on bulk RNA-seq gene expression profile data to screen for differentially expressed genes. To further identify candidate markers associated with M1 and M2 macrophages, we intersected these genes and obtained 14 and 17 candidate marker genes for M1 and M2 macrophages, respectively.

Furthermore, TFs from multiple databases were used to construct a multi-factor regulatory network of candidate markers for M1 and M2 macrophages. In the multi-factor regulatory network of M1 macrophages, there were 6 M1 macrophage candidate markers, 159 TFs, and 48 miRNAs. The multi-factor regulatory network of M2 macrophages included 13 M2 macrophage candidate markers, 191 TFs, and 182 miRNAs.

Consistency clustering of patients was performed based on the expression of M1 and M2 macrophage candidate markers, and patients with OC were stratified. The gene expression among patients with different subtypes showed significant differences. In total, 167 and 851 differentially expressed genes were identified in patients with the M1 and M2 macrophage subtypes, respectively.

We used machine learning to filter out differentially expressed genes to explore new drug intervention targets to provide personalized treatment for stratified patients. In total, 15 M1 and M2 macrophage-specific markers were identified. Meanwhile, we found that these markers were closely related to the sensitivity of standard chemotherapy drugs, such as *MXRA8* expression level and dasatinib sensitivity, which were significantly negatively correlated. MXRA8 is a transmembrane protein that can bind to alpha viruses such as chikungunya virus and allow the virus to enter cells [36]. In contrast, *USP34* expression level and afatinib sensitivity were significantly correlated negatively. *USP34* encodes a deubiquitinase [37]. This result is similar to the experimental results of previous studies [38,39]. We conducted a preliminary analysis of the regulatory relationships between the top 10 TFs and miRNAs in the multifactor regulatory network of M1 and M2 macrophages with *MXRA8* or *USP34*. The results showed that these TFs and miRNAs were positively correlated with the expression levels of MXRA8 or USP34, suggesting that they may play a role in promoting the expression of these markers.

To further confirm the reliability of these results, we conducted in vitro experiments to validate the specific markers, *MXRA8* and *USP34*, in M1 and M2 macrophages. The results confirmed that OC patients with high expression levels of these two genes were resistant to dasatinib and afatinib, respectively.

This study has some limitations. First, our analysis is based on previously publicly available data, a retrospective study requiring more clinical real data for prospective analysis and validation. Second, we only conducted in vitro experimental verification of the experimental results. In the future, we need to further conduct in vivo experiments to validate our analysis results, which will help to validate our findings and explore new drug intervention targets for patients with OC.

5. Conclusion

This study identified candidate markers for M1 and M2 macrophages in patients with serous OC. Based on these candidate markers we explored M1 and M2 macrophage subtypes in patients with serous OC and identified specific markers for M1 and M2 macrophages. The potential therapeutic compounds with specific markers were explored using drug sensitivity prediction analyses and in vitro experiments. Discovering these potential therapeutic compounds promotes an understanding of the underlying mechanisms of serous OC and inspires more effective treatment methods.

CRediT authorship contribution statement

Fei Teng: Conceptualization. **Hong Wei:** Investigation. **Dehong Che:** Formal analysis. **Kuo Miao:** Methodology. **Xiaoqiu Dong:** Data curation.

Data availability

The datasets analyzed during the current study are available in the Gene Expression Omnibus (GEO) and The Cancer Genome Atlas (TCGA) repository. The web link of GEO is https://www.ncbi.nlm.nih.gov/geo/, datasets in GEO includes GSE26712. The web link of TCGA is https://portal.gdc.cancer.gov/repository.

Ethics approval

This study was performed in line with the principles of the Declaration of Helsinki. Approval was granted by the Clinical Research Ethics Committee of the Second Affiliated Hospital of Harbin Medical University (KY2024-155).

Funding

This work was supported by Natural Science Foundation of Heilongjiang Province, China (Grant NO. LH2022H033).

Declaration of competing interest

The authors declare that they have no known competing financial interests or personal relationships that could have appeared to influence the work reported in this paper.

Acknowledgements

The authors thank TCGA, PubMed, and GEO for data access. We would like to thank Editage (www.editage.cn) for the English language editing.

Appendix A. Supplementary data

Supplementary data to this article can be found online at https://doi.org/10.1016/j.heliyon.2025.e42429.

References

[1] F. Bray, J. Ferlay, I. Soerjomataram, R.L. Siegel, L.A. Torre, A. Jemal, Global cancer statistics 2018: GLOBOCAN estimates of incidence and mortality worldwide for 36 cancers in 185 countries, CA Cancer J. Clin. 68 (6) (2018) 394–424.
[2] A. Khodavandi, F. Alizadeh, A.F.A. Razis, Association between dietary intake and risk of ovarian cancer: a systematic review and meta-analysis, Eur. J. Nutr. 60 (4) (2021) 1707–1736.
[3] Z. Li, L. Huang, L. Wei, B. Zhang, S. Zhong, Y. Ou, C. Wen, S. Huang, KCNH3 predicts poor prognosis and promotes progression in ovarian cancer, OncoTargets Ther. 13 (2020) 10323–10333.
[4] H. Angell, J. Galon, From the immune contexture to the Immunoscore: the role of prognostic and predictive immune markers in cancer, Curr. Opin. Immunol. 25 (2) (2013) 261–267.
[5] A. Ghoneum, S. Almousa, B. Warren, A.Y. Abdulfattah, J. Shu, H. Abouelfadl, D. Gonzalez, C. Livingston, N. Said, Exploring the clinical value of tumor microenvironment in platinum-resistant ovarian cancer, Semin. Cancer Biol. 77 (2021) 83–98.
[6] Z. Husain, P. Seth, V.P. Sukhatme, Tumor-derived lactate and myeloid-derived suppressor cells: linking metabolism to cancer immunology, OncoImmunology 2 (11) (2013) e26383.
[7] D.S. Vinay, E.P. Ryan, G. Pawelec, W.H. Talib, J. Stagg, E. Elkord, T. Lichtor, W.K. Decker, R.L. Whelan, H. Kumara, et al., Immune evasion in cancer: mechanistic basis and therapeutic strategies, Semin. Cancer Biol. 35 (Suppl) (2015) S185–S198.
[8] A. Ene-Obong, A.J. Clear, J. Watt, J. Wang, R. Fatah, J.C. Riches, J.F. Marshall, J. Chin-Aleong, C. Chelala, J.G. Gribben, et al., Activated pancreatic stellate cells sequester CD8+ T cells to reduce their infiltration of the juxtatumoral compartment of pancreatic ductal adenocarcinoma, Gastroenterology 145 (5) (2013) 1121–1132.
[9] H. Zhang, R. Jiang, J. Zhou, J. Wang, Y. Xu, H. Zhang, Y. Gu, F. Fu, Y. Shen, G. Zhang, et al., CTL attenuation regulated by PS1 in cancer-associated fibroblast, Front. Immunol. 11 (2020) 999.
[10] O.J. Finn, Human tumor antigens yesterday, today, and tomorrow, Cancer Immunol. Res. 5 (5) (2017) 347–354.
[11] H. Kasashima, M. Yashiro, H. Kinoshita, T. Fukuoka, T. Morisaki, G. Masuda, K. Sakurai, N. Kubo, M. Ohira, K. Hirakawa, Lysyl oxidase-like 2 (LOXL2) from stromal fibroblasts stimulates the progression of gastric cancer, Cancer Lett. 354 (2) (2014) 438–446.
[12] A. Orimo, R.A. Weinberg, Stromal fibroblasts in cancer: a novel tumor-promoting cell type, Cell Cycle 5 (15) (2006) 1597–1601.
[13] S. Reinartz, T. Schumann, F. Finkernagel, A. Wortmann, J.M. Jansen, W. Meissner, M. Krause, A.M. Schworer, U. Wagner, S. Muller-Brusselbach, et al., Mixed-polarization phenotype of ascites-associated macrophages in human ovarian carcinoma: correlation of CD163 expression, cytokine levels and early relapse, Int. J. Cancer 134 (1) (2014) 32–42.
[14] M. Yin, X. Li, S. Tan, H.J. Zhou, W. Ji, S. Bellone, X. Xu, H. Zhang, A.D. Santin, G. Lou, et al., Tumor-associated macrophages drive spheroid formation during early transcoelomic metastasis of ovarian cancer, J. Clin. Investig. 126 (11) (2016) 4157–4173.
[15] J.W. Pollard, Tumour-educated macrophages promote tumour progression and metastasis, Nat. Rev. Cancer 4 (1) (2004) 71–78.
[16] H. Li, F. Luo, X. Jiang, W. Zhang, T. Xiang, Q. Pan, L. Cai, J. Zhao, D. Weng, Y. Li, et al., CircITGB6 promotes ovarian cancer cisplatin resistance by resetting tumor-associated macrophage polarization toward the M2 phenotype, J Immunother Cancer 10 (3) (2022).
[17] C.W. Wanderley, D.F. Colon, J.P.M. Luiz, F.F. Oliveira, P.R. Viacava, C.A. Leite, J.A. Pereira, C.M. Silva, C.R. Silva, R.L. Silva, et al., Paclitaxel reduces tumor growth by reprogramming tumor-associated macrophages to an M1 profile in a TLR4-dependent manner, Cancer Res. 78 (20) (2018) 5891–5900.
[18] C. Yan, K. Li, F. Meng, L. Chen, J. Zhao, Z. Zhang, D. Xu, J. Sun, M. Zhou, Integrated immunogenomic analysis of single-cell and bulk tissue transcriptome profiling unravels a macrophage activation paradigm associated with immunologically and clinically distinct behaviors in ovarian cancer, J. Adv. Res. 44 (2023) 149–160.
[19] T. Miyamoto, R. Murakami, J. Hamanishi, K. Tanigaki, Y. Hosoe, N. Mise, S. Takamatsu, Y. Mise, M. Ukita, M. Taki, et al., B7-H3 suppresses antitumor immunity via the CCL2-CCR2-M2 macrophage Axis and contributes to ovarian cancer progression, Cancer Immunol. Res. 10 (1) (2022) 56–69.
[20] J. Qian, S. Olbrecht, B. Boeckx, H. Vos, D. Laoui, E. Etlioglu, E. Wauters, V. Pomella, S. Verbandt, P. Busschaert, et al., A pan-cancer blueprint of the heterogeneous tumor microenvironment revealed by single-cell profiling, Cell Res. 30 (9) (2020) 745–762.
[21] I. Tirosh, B. Izar, S.M. Prakadan, M.H. Wadsworth, D. Treacy, J.J. Trombetta, A. Rotem, C. Rodman, C. Lian, G. Murphy, et al., Dissecting the multicellular ecosystem of metastatic melanoma by single-cell RNA-seq, Science 352 (6282) (2016) 189–196.
[22] D. Lambrechts, E. Wauters, B. Boeckx, S. Aibar, D. Nittner, O. Burton, A. Bassez, H. Decaluwe, A. Pircher, K. Van den Eynde, et al., Phenotype molding of stromal cells in the lung tumor microenvironment, Nat. Med. 24 (8) (2018) 1277–1289.

[23] J. Peng, B.F. Sun, C.Y. Chen, J.Y. Zhou, Y.S. Chen, H. Chen, L. Liu, D. Huang, J. Jiang, G.S. Cui, et al., Single-cell RNA-seq highlights intra-tumoral heterogeneity and malignant progression in pancreatic ductal adenocarcinoma, Cell Res. 29 (9) (2019) 725–738.
[24] N. Aizarani, A. Saviano, Mailly L. Sagar, S. Durand, J.S. Herman, P. Pessaux, T.F. Baumert, D. Grun, A human liver cell atlas reveals heterogeneity and epithelial progenitors, Nature 572 (7768) (2019) 199–204.
[25] A.S. Venteicher, I. Tirosh, C. Hebert, K. Yizhak, C. Neftel, M.G. Filbin, V. Hovestadt, L.E. Escalante, M.L. Shaw, C. Rodman, et al., Decoupling genetics, lineages, and microenvironment in IDH-mutant gliomas by single-cell RNA-seq, Science 355 (6332) (2017).
[26] V. Hovestadt, K.S. Smith, L. Bihannic, M.G. Filbin, M.L. Shaw, A. Baumgartner, J.C. DeWitt, A. Groves, L. Mayr, H.R. Weisman, et al., Resolving medulloblastoma cellular architecture by single-cell genomics, Nature 572 (7767) (2019) 74–79.
[27] S.V. Puram, I. Tirosh, A.S. Parikh, A.P. Patel, K. Yizhak, S. Gillespie, C. Rodman, C.L. Luo, E.A. Mroz, K.S. Emerick, et al., Single-cell transcriptomic analysis of primary and metastatic tumor ecosystems in head and neck cancer, Cell 171 (7) (2017) 1611–1624, e1624.
[28] T. Bonome, D.A. Levine, J. Shih, M. Randonovich, C.A. Pise-Masison, F. Bogomolniy, L. Ozbun, J. Brady, J.C. Barrett, J. Boyd, et al., A gene signature predicting for survival in suboptimally debulked patients with ovarian cancer, Cancer Res. 68 (13) (2008) 5478–5486.
[29] S. Olbrecht, P. Busschaert, J. Qian, A. Vanderstichele, L. Loverix, T. Van Gorp, E. Van Nieuwenhuysen, S. Han, A. Van den Broeck, A. Coosemans, et al., High-grade serous tubo-ovarian cancer refined with single-cell RNA sequencing: specific cell subtypes influence survival and determine molecular subtype classification, Genome Med. 13 (1) (2021) 111.
[30] M. Kanehisa, M. Furumichi, Y. Sato, M. Kawashima, M. Ishiguro-Watanabe, KEGG for taxonomy-based analysis of pathways and genomes, Nucleic Acids Res. 51 (D1) (2023) D587–D592.
[31] M. Kanehisa, Y. Sato, KEGG Mapper for inferring cellular functions from protein sequences, Protein Sci. 29 (1) (2020) 28–35.
[32] C. Zhou, J. Ji, Q. Cai, M. Shi, X. Chen, Y. Yu, Z. Zhu, J. Zhang, MTA2 enhances colony formation and tumor growth of gastric cancer cells through IL-11, BMC Cancer 15 (2015) 343.
[33] S.C. Mok, T. Bonome, V. Vathipadiekal, A. Bell, M.E. Johnson, K.K. Wong, D.C. Park, K. Hao, D.K. Yip, H. Donninger, et al., A gene signature predictive for outcome in advanced ovarian cancer identifies a survival factor: microfibril-associated glycoprotein 2, Cancer Cell 16 (6) (2009) 521–532.
[34] E.A. Eisenhauer, Real-world evidence in the treatment of ovarian cancer, Ann. Oncol. 28 (suppl_8) (2017) viii61–viii65.
[35] U.A. Matulonis, A.K. Sood, L. Fallowfield, B.E. Howitt, J. Sehouli, B.Y. Karlan, Ovarian cancer, Nat. Rev. Dis. Primers 2 (2016) 16061.
[36] K.E. Simpson, C.A. Staikos, K.L. Watson, R.A. Moorehead, Loss of MXRA8 delays mammary tumor development and impairs metastasis, Int. J. Mol. Sci. 24 (18) (2023).
[37] C. Lin, J. Xia, Z. Gu, Y. Meng, D. Gao, S. Wei, Downregulation of USP34 inhibits the growth and migration of pancreatic cancer cells via inhibiting the PRR11, OncoTargets Ther. 13 (2020) 1471–1480.
[38] X. Shen, X. Jin, S. Fang, J. Chen, EFEMP2 upregulates PD-L1 expression via EGFR/ERK1/2/c-Jun signaling to promote the invasion of ovarian cancer cells, Cell. Mol. Biol. Lett. 28 (1) (2023) 53.
[39] J. Liu, Y. Liu, C. Yang, J. Liu, J. Hao, Comprehensive analysis for the immune related biomarkers of platinum-based chemotherapy in ovarian cancer, Transl Oncol 37 (2023) 101762.